

# Raising the Bar of AI-generated Image Detection with CLIP

Davide Cozzolino<sup>1</sup> Giovanni Poggi<sup>1</sup> Riccardo Corvi<sup>1</sup> Matthias Nießner<sup>2</sup> Luisa Verdoliva<sup>1,2</sup>

<sup>1</sup>University Federico II of Naples <sup>2</sup>Technical University of Munich

## Abstract

Aim of this work is to explore the potential of pre-trained vision-language models (VLMs) for universal detection of AI-generated images. We develop a lightweight detection strategy based on CLIP features and study its performance in a wide variety of challenging scenarios. We find that, unlike previous belief, it is neither necessary nor convenient to use a large domain-specific dataset for training. On the contrary, by using only a handful of example images from a single generative model, a CLIP-based detector exhibits a surprising generalization ability and high robustness across several different architectures, including recent commercial tools such as Dalle-3, Midjourney v5, and Firefly. We match the SoTA on in-distribution data, and improve largely above it in terms of generalization to out-of-distribution data (+6% in terms of AUC) and robustness to impaired/laundered data (+13%). Our project is available at <https://grip-unina.github.io/ClipBased-SyntheticImageDetection/>

## 1. Introduction

Synthetic images have by now left the research laboratories and are flooding the real world. The latest versions of popular image editing tools, such as Adobe Photoshop and Microsoft Paint, come with easy-to-use AI-powered generative tools that allow even novice users to edit and generate visual content at will. Thanks to diffusion-based generative models, it is not only the quality of the images generated that has improved enormously, but also the flexibility in using these tools. By issuing a few textual commands, it is possible to easily obtain the desired image. While this represents a great opportunity for visual art applications, it is also the paradise of disinformation professionals who can design their attacks with unprecedented power and flexibility [5, 8, 25]. And, of course, a nightmare for all those trying to combat the spread of fake news and orchestrated disinformation campaigns: journalists, fact-checkers, law enforcement agencies, governments. Therefore, there is high demand for automatic tools that help establishing the authenticity of a media asset.

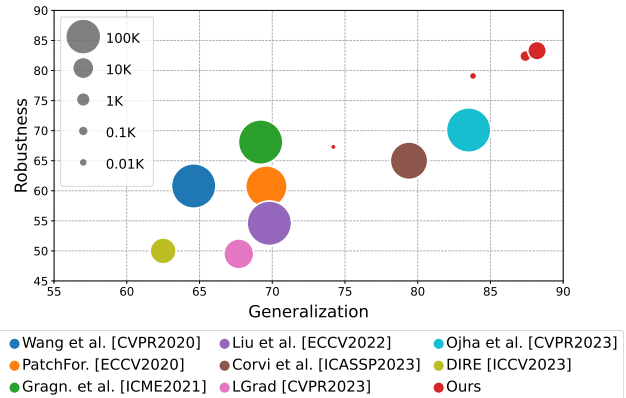


Figure 1. Area Under ROC Curve (AUC %) on unseen synthetic generators ( $x$ -axis) and on post-processed data ( $y$ -axis). The first number measures the generalization ability of the detector, the second its robustness to possible impairments. Circle area proportional to training set size. The performance is measured over 18 different synthetic models. Our CLIP-based detector largely outperforms all SOTA methods with very limited training data.

It is well known that each synthesis model leaves its own peculiar traces in all generated images, subtle traces that give rise to so called *artificial fingerprints*, that can be exploited for forensic analyses [49, 77]. This was first observed for methods based on generative adversarial networks (GAN) [22, 79] but holds with obvious differences for all generation approaches, including the more recent diffusion models (DM) [13]. One of the main challenges for current forensic detectors is the ability to generalize to new and unseen generative methods. Indeed, the in-distribution (ID) scenario, with perfectly aligned training and test set, is rarely met in practice. Test images are often generated by new approaches, unseen architectures, or even known architectures re-trained under different conditions, all different flavors of the out-of-distribution (OOD) scenario. In addition, most of the times, images are downloaded from some social networks, where they undergo transformations such as compression and resizing (even multiple times), processes that tend to wash out the tiny traces so precious for detection.

In [71], it is shown that training diversity and intense

augmentation are crucial for generalization. A ResNet-50 detector is trained on a single but very diverse dataset of about 360k ProGAN images [40]. Results on OOD images generated by other GAN-based generators turned out to be surprisingly good. The authors themselves, however, suggest that structural similarities between GAN-based generators are the likely reason for such good performance. Indeed, results are not equally good on images generated by recent diffusion-based methods, which present somewhat different generation artifacts [14].

Generalizing to OOD data is a major issue in deep learning and has been the object of intense research in latest years. In this context, the advent of large pre-trained vision-language models has brought about a number of new solutions and exciting results. These models have been shown to be excellent zero-shot and few-shot learners in many diverse applications, such as image classification [59, 78], detection [26, 53] and segmentation [74, 81]. Recently, there have been attempts to exploit the power of VLMs to detect synthetic images [2, 56, 66]. For example, in [56] CLIP (Contrastive Language-Image Pre-Training) [59] is used as a pre-trained feature extractor, and a classifier is then trained on the 360k-image ProGAN dataset proposed in [71], with the same augmentation strategy. With respect to [71] based on Resnet50, the performance improves significantly, especially on images generated by diffusion models, showing a very good generalization ability.

In this work we explore in depth the potential of CLIP for image forensics, propose new decision strategies, and carry out an extensive experimental analysis in challenging real-world scenarios involving a large number of generative models. We find that CLIP-based methods show impressive generalization ability and very good robustness, resulting in large performance improvements compared to the state of the art. To obtain such results we avoid any intensive training on domain-specific data, which may introduce unwanted biases and undermine the descriptive power of CLIP features. Instead, we rely on a small number of paired real/fake images with the same textual description and use their CLIP features to model the decision space. Synthetic images come from a single generator but work well with all other tested data sources. The top performance is obtained with just 1000 to 10000 paired images. Moreover, only minor decays are observed when this number reduces to 100 or even 10 (see Fig. 1).

In summary, the key contributions of this work are as follows:

- We show that CLIP features achieve excellent generalization: by exploiting only a handful of examples, not even belonging to the generator under test, the performances are comparable to those of intensively trained solutions.
- We carry out a large set of experiments on diverse synthetic generators and in very challenging conditions and

are able to achieve the best performance (on average). Our experiments make clear that the features extracted are at least partially orthogonal to those explored by previous methods mostly oriented to extract low-level features.

## 2. Related work

There is an extensive literature on synthetic image detection, mostly concerning images created by generative adversarial networks (GANs) and, more recently, by diffusion models (DMs). Some methods look for visible errors, such as asymmetries in faces, wrong perspective, odd shadows [28, 29, 51]. However, with the rapid progress in image synthesis technology, this kind of problems are solved quickly and appear more and more rarely in modern generation methods. Hence, we will focus on methods that exploit “invisible” forensic traces, working either in the spatial or the frequency domain. Then we will briefly review the most recent approaches that exploit multimodal features.

**Spatial domain methods.** Despite their high visual quality, synthetic images carry with them distinctive traces of the generation process that enable detection and even model identification [49, 77]. In fact, each generation model inserts a sort of digital fingerprint into all the images created, which depends on its architectural and training details. This fingerprint can be easily estimated. Given an adequate number of images generated by the target model, typically a few hundred, it is sufficient to average their noise residuals, extracted through simple denoisers [49] or more sophisticated deep learning-based methods [47, 67]. Detectors based on digital fingerprints can be regarded as “few-shot”, as they can deal with new models based on just a few example images. Other few-shot solutions have been proposed lately in this field [15, 21, 36, 50]. However, they all require some prior knowledge of the target models, even if limited to a few images, so they fit a strictly in-distribution (ID) scenario. In contrast, our work aims to generalize to new and previously unseen models, and therefore fits into an out-of-distribution (OOD) scenario.

Good generalization is a key requirement of synthetic image detectors. Towards this end, it is important to increase diversity in training, which can be pursued by suitable augmentation, by including a large number of different categories [71], or even by model ensembling [48]. Other studies suggest to work on local patches [9] or combine global spatial information with local features [38]. In [33] it is shown that to preserve the subtle high-frequency forensic traces, one should avoid any downsampling in the first layers of the network. With the same aim, [69] proposes to work on noise residuals rather than the original images, by extracting the gradients with a pre-trained CNN. In [12] a systematic study is carried out on transferable forensic features that allows easier generalization.

The above investigations and proposals, however, only consider GAN-based generators. Some very recent works extend the analyses to latest generation approaches. [14] shows that detectors designed for GAN images have a hard time generalizing to DM images, especially in the presence of common post-processing steps such as compression and resizing. Furthermore, they are unable to select an adequate decision threshold without the help of some calibration data from the model under test. On the other hand, [24] shows that it is possible to achieve decent performance by continuously re-training the detector on images from new generators, as long as the latter share some architectural components with the known ones. In [72], inspired to previous work on GAN images [1], a detector specifically tailored to DM images is proposed. Images are projected in a latent space and reconstructed with known models to study their features. While promising, the approach refers to specific architectures, hence an ID scenario, and has been tested on a limited set of diffusion generative models. In the present work, instead, we do not make any assumptions on the test data and include a large variety of both GAN and DM generators including OOD images, and realistic high-resolution images generated by recent diffusion models.

**Frequency domain methods.** GAN-image artifacts are more easily spotted in the frequency domain and are clearly visible in the artificial fingerprint spectra [22, 23, 31]. In fact, they are caused by the up-sampling operations used in the generator, which give rise to regular spatial patterns and strong peaks in the Fourier domain. Interestingly, the awareness of such weakness has prompted the design of new architectures, like StyleGAN3 [43], which explicitly avoid aliasing and reduce the above mentioned peaks. In addition to such obvious artifacts, the spectral content of GAN images and real images is also known to differ significantly in the medium and high frequencies. Likewise, clear differences in the radial and angular spectral distributions of the DM and real images were observed [13, 75]. Furthermore, it is worth observing that DM images also may present spectral peaks (see Fig. 5).

Of course, frequency domain traces can be used to train simple detectors for ID images. Even more interestingly, some authors [37, 79] replicate and modify the synthesis process of known generators by introducing a series of small architectural changes in order to learn to manage also OOD test images. A major problem with spectral traces is that they can be easily weakened by laundering operations, both innocent (e.g., image resizing) and malicious counterforensic methods [11, 20]. Likewise, attackers can easily embed artificial spectral traces in a real image to make it appear as synthetic. This is a more general problem of low-level traces, which can be attacked in both ways and through a number of ingenious methods. We will show that our approach is indeed immune to such attacks and can handle a

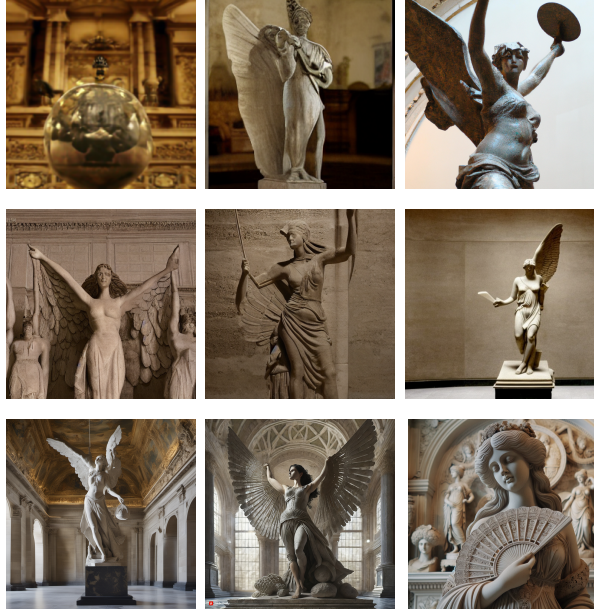


Figure 2. Examples of synthetic images from generators used in our experiments. From left to right, Top: GLIDE [55], Latent Diffusion [60], DALL-E 2 [60]. Middle: Stable Diffusion 1.3, Stable Diffusion 1.4, Stable Diffusion 2.1 [62]. Bottom: Stable Diffusion XL [58], Adobe Firefly [30], DALL-E 3 [6].

variety of distribution shift.

**Exploiting multimodal features.** The introduction of large language models has elicited intense work in the vision community on trying to exploit large models trained using both images and text [78, 80]. In image forensics, however, traditionally oriented to the analysis of low-level features, there has been very little work in this direction. Only a few papers [2, 56, 66] have tried exploiting pre-trained visual models for the detection of AI-generated images. All of them rely on variants of CLIP, however only in [56] it is pursued generalization to OOD data, by nearest neighbor and linear probing in the CLIP feature space. To this end, a large dataset of fake and real images is used to train the classifier. In this work we make a further step in this direction and show that better performance can be achieved even using much less data.

### 3. Datasets and metrics

The main objective of this work is to study the generalization ability of CLIP-based and conventional methods, that is, assess how the detectors behave on data never seen before, of different provenance, and possibly impaired by various forms of post-processing. Therefore, we consider a very large test dataset and try to avoid any possible biases in the experimental validation.

Tab. 1 lists all the generation models used in testing.

They are grouped in three families: GAN-based (ProGAN, StyleGAN2, StyleGAN3, StyleGAN-T, GigaGAN), DM-based (Score-SDE, ADM, GLIDE, eDiff-I, Latent and Stable Diffusion, DiT, DeepFloyd-IF, Stable Diffusion XL) and commercial tools (DALL-E 2, DALL-E 3, Midjourney v5 and Adobe Firefly), which includes some recent text-driven methods available on-line, whose architecture is not always disclosed. These models cover the different generation modalities commonly adopted in this field: unconditional (u), conditional (c), and text-to-image (t), reported in second column of the table.

The last column reports the resolution of the images in the dataset. The central columns, instead, indicate which datasets of real images have been considered to carry out the detection experiments. These have been carefully selected to avoid all foreseeable biases. For example, when testing on synthetic images generated by ProGAN, we use as real counterparts images drawn from the LSUN dataset on which the ProGAN model was trained. Therefore, if LSUN images shared all the same defect (say, a red "LSUN" label in a corner) the ProGAN images should spot the same defect, which could not be used to spoil detection performance. This hilarious example should not hide the importance of the problem, as biases are way too common in experiments and not always so easy to avoid. In other cases, for example when text-driven commercial tools with undisclosed training details are used, we relied on a dataset recently proposed in [4]. Pristine and synthetic images with similar semantic content are built by extracting textual descriptions from a real dataset (RAISE [16]) and then using them as prompt for generating synthetic ones. Overall, we selected 32,000 real and fake images for testing, which will form the dataset used in all forthcoming experiments. To consider a more realistic scenario, we also consider datasets with post-processing operations that simulate images shared over social networks. In particular, we apply random cropping, resizing and JPEG compression at different quality levels. More details on the dataset can be found in the supplemental material, here we only show a few examples in Fig. 2.

To measure performance, we consider three metrics. The area under the receiver-operating curve (AUC), and the average precision (AP), equal to the area under the precision-recall curve, are both threshold-independent. The Accuracy instead, given by the number of correct predictions divided by the number of tested images, depends on the decision threshold. We use always a fixed threshold equal to 0.5, which fits a realistic scenario with no prior information on the data under test to carry out proper calibration.

#### 4. CLIP for synthetic image detection

We propose a simple procedure to tell apart real images from synthetic images based on features extracted from the

Generator	modality	LSUN [76]	FFHQ [41]	ImageNet [18]	COCO [46]	LAION [64]	RAISE [16]	Resolution
ProGAN [40]	u	✓						256 <sup>2</sup>
StyleGAN2 [42]	u	✓	✓					256 <sup>2</sup> -1024 <sup>2</sup>
StyleGAN3 [43]	u		✓					256 <sup>2</sup> -1024 <sup>2</sup>
StyleGAN-T [63]	t				✓			512 <sup>2</sup>
GigaGAN [39]	c,t			✓		✓		256 <sup>2</sup> ,512 <sup>2</sup>
Score-SDE [68]	u		✓					256 <sup>2</sup>
ADM [19]	u,c	✓		✓				256 <sup>2</sup>
GLIDE [55]	t				✓		✓	256 <sup>2</sup>
eDiff-I [3]	t				✓			256 <sup>2</sup> ,1024 <sup>2</sup>
Latent Diff. [61]	u,c,t	✓	✓	✓	✓			256 <sup>2</sup>
Stable Diff. [62]	t					✓	✓	256 <sup>2</sup> -768 <sup>2</sup>
DiT [57]	c			✓				256 <sup>2</sup> ,512 <sup>2</sup>
DeepFloyd-IF [44]	t				✓			1024 <sup>2</sup>
Stable Diff. XL [58]	t						✓	1024 <sup>2</sup>
DALL-E 2 [60]	t						✓	1024 <sup>2</sup>
DALL-E 3 [6]	t						✓	1024 <sup>2</sup>
Midjourney V5 [52]	t						✓	1024 <sup>2</sup> -1100 <sup>2</sup>
Adobe Firefly [30]	t						✓	2032 <sup>2</sup> -2048 <sup>2</sup>

Table 1. Image generators used in our experiments: GAN-based, DM-based, and commercial tools with models not always disclosed. For unconditional (u) and conditional (c) models, to prevent biases, the real images used in test come from the same datasets used to train the generator. Image resolution varies from 256×256 to 2048×2048.

image encoder of CLIP ViT L/14. The design of the detector consists of the following four steps:

1. collect  $N$  real images  $\{R_1, \dots, R_N\}$  with the corresponding captions  $\{t_1, \dots, t_N\}$ ;
2. use the captions to feed a text-driven image generator,  $G(\cdot)$ , so as to obtain  $N$  synthetic images  $\{F_1, \dots, F_N\}$  with  $F_i = G(t_i)$ . We have now  $N$  real / fake pairs that share the same textual description;
3. feed CLIP with the  $N$  real and  $N$  fake images and collect the corresponding feature vectors  $\{r_1, \dots, r_N\}$  and  $\{f_1, \dots, f_N\}$  extracted at the output of the next-to-last layer, with  $r_i = \text{CLIP}(R_i)$  and  $f_i = \text{CLIP}(F_i)$ ;
4. use the  $N+N$  feature vectors to design a linear SVM classifier.

If the real images have low-quality associated captions, or no caption at all, these can be easily generated by a dedicated tool such as BLIP [45]. Real and fake images are coupled to avoid possible semantic biases, which proves beneficial when the number of images is very small, *e.g.*,  $N = 10$ . We chose to extract features from the next-to-last layer rather than the last layer based on the results of preliminary experiments and, in the same way, we selected SVM among a set of candidate simple classifiers. All these preliminary experiments and their results are described in the supplemental material.

In the following, we analyze the performance of the proposed detector as a function of the main design choices and

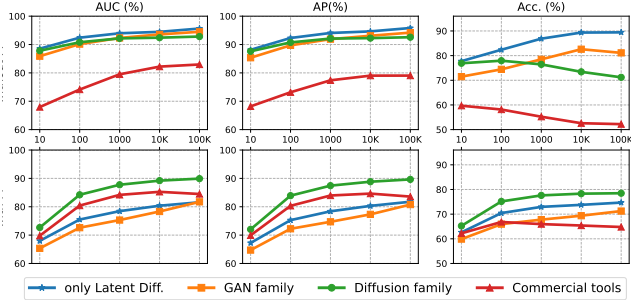


Figure 3. Performance of the CLIP-based detector as a function of the number of real and synthetic images in the reference set. We show AUC, AP and Accuracy on the original dataset (Top) and on post-processed images that simulate a realistic scenario (Bottom).

experimental conditions.

#### 4.1. Influence of the reference set size

We begin with investigating the role of the most important parameter of the proposed detector, the number of real / synthetic samples  $N$  in the reference set, that in this experiment includes COCO real images and Latent Diffusion generated ones. Fig. 3 shows results for  $N$  varying from 10 to 100k in log scale. The results are presented in terms of AUC, AP, and Accuracy. When  $N$  is less than 10k, we perform several runs with different sets of images and report the average metrics, e.g. for  $N$  equals to 1k, we show the average on 10 runs.

Let us focus first on the top row, showing results on images that have been neither re-compressed nor resized. In this simpler scenario, AUC and AP are extremely high, always above 85% for all known families of synthetic images (GAN, Diffusion) and somewhat worse for images generated by commercial tools. Especially remarkable is the fact that very good results are obtained already with as few as 10+10 reference images, showing this lightweight solution to be fully viable. The performance improves with  $N$ , growing by up to 5-10 percent points at the  $N = 10k$  plateau. We observe, in passing, that AUC and AP curves are very similar, as always happens when they approach 100%, hence we drop the latter for brevity in further experiments.

In the rightmost figure, we see that unlike AUC and AP, accuracy does not always improve with increasing  $N$ . This is because AUC and AP are integral threshold-independent metrics. They tell us how well a method could do with a perfectly calibrated threshold. On the contrary, accuracy depends critically on the selected threshold which, lacking any prior knowledge, is set to 0.5. For Latent and GAN, 0.5 is a good threshold, and accuracy improves as the classifier does. Instead, for Diffusion and Commercial, the optimal threshold grows farther from 0.5 as  $N$  increases and the accuracy decreases significantly. So there is a trade-off be-

Datasets	augm.	GAN family	Diffusion family	Commerc. tools	AVG
COCO + Latent		93.9	93.3	81.7	89.6
COCO + Latent	✓	84.8	91.0	87.6	87.8
COCO + ProGAN		95.0	90.0	65.6	83.5
COCO + ProGAN	✓	92.3	90.1	82.3	88.2
LSUN + Latent		87.0	82.7	65.6	78.5
LSUN + Latent	✓	86.8	79.9	80.3	82.4
LSUN + ProGAN		93.8	79.2	44.7	72.6
LSUN + ProGAN	✓	95.7	82.7	67.5	82.0

Table 2. Performance of the CLIP-based detector for various real/fake combinations, with and without augmentation.

tween optimality and robustness in our truly OOD scenario, where no calibration data exist (it is very unlikely that we know exactly which is the generator of the data under test). On the other hand, if we had data from the target class, even just 10 images, we could use them to design and *ad hoc* classifier.

The bottom row of the figure shows results for images that have been compressed and/or resized. As expected, performance degrades somewhat in this scenario, but continues to be very good, with AUC between 75% and 90% and accuracy between 65% and 80% at  $N=10k$ . These are excellent results, much beyond the current state of the art, as we will show later. In this case, using only 10+10 images seems not to be advisable but the performance is near-optimal already at  $N=100$ .

#### 4.2. Influence of the reference set content

We discovered that not only the size but also the quality of the reference set images impacts heavily on performance. This probably does not need proof if we think about a very small reference set, like 10+10 images, where low quality or low diversity would spell catastrophe. However, something similar happens also when a larger reference set is used. Tab. 2 shows the results in terms of AUC obtained using various combination of real and synthetic images in the reference set, that is,  $(\text{Real}, \text{Synth}) \in \{\text{COCO}, \text{LSUN}\} \times \{\text{Latent}, \text{ProGAN}\}$ , with and without augmentation. In all cases, the reference set has size 10000+10000. Results are clearly affected by the specific combination. Indeed, there is a marked impairment when the LSUN dataset is used instead of COCO to draw the real samples and also, to a lesser extent, when ProGAN is used instead of Latent for the synthetic images. We conjecture that both LSUN and ProGAN are not diverse enough to describe adequately the decision domain. Moreover, LSUN has several polarizations not included in COCO, the images of LSUN represent only few well-defined categories, have all the same size, and are compressed most of them with the same quality factor. In Tab. 2, we see that data augmentation only marginally reduces the effects of the used dataset.

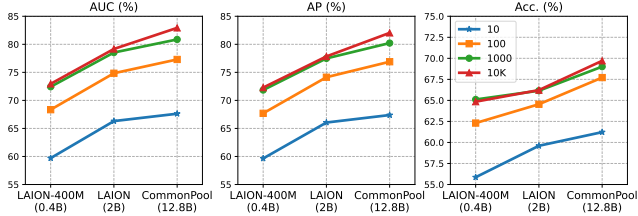


Figure 4. Performance of the CLIP-based detector as a function of the pre-training. We show AUC, AP and Accuracy on post-processed images for models pre-trained on LAION-400M (0.4B images), LAION (2B) and CommonPool (12.8B).

### 4.3. Influence of pre-training

We experimented also with various versions of CLIP ViT L/14 [35], trained on different datasets, observing significant changes in performance. Fig. 4 shows, the AUC, AP and Accuracy averaged on all families of models as a function of the pre-training dataset. Each curve refers to a different value of  $N$  and we consider only the case of post processed images for brevity. For both metrics and all values of  $N$  there is a steady increase in performance as larger and larger datasets are used for pre-training, from LAION-400M (0.4B images) [64], to LAION (2B) [65], to CommonPool (12.8B) [32]. Overall, from smallest to largest dataset there is a ten point improvement! This comes to confirm, if ever necessary, the importance of pre-training a large VLM on the largest possible collection of varied images to acquire greater descriptive power for all kinds of applications.

### 4.4. Beyond low-level forensic traces

As already highlighted in the Introduction, forensic classifiers typically rely on subtle low-level artifacts. These can be seen more clearly in the frequency domain, where they appear as strong peaks. In this subsection we report on some initial analysis aimed at understanding whether the CLIP-based detector also relies on this type of traces or it exploits different information. To this end, we consider the high resolution  $1024 \times 1024$ -pixel images generated by Stable Diffusion XL and resize them to  $256 \times 256$ . Fig. 5 shows, on the right, the high and low-resolution images (top) together with their spectra (bottom). We observe that after resizing, the spectral artifacts have completely disappeared. In fact, these traces are caused by the aliasing effect of the upsampling filters, which can be removed by proper decimation. We run our detector on 1000 original and resized synthetic images, obtaining in both cases the same True Positive Rate (TPR) of 43% (note that the True Negative Rate (TNR) for these images is 97%).

We also carry out a complementary experiment where we take real images and pass them through the generative architecture of Stable Diffusion which acts as an autoen-

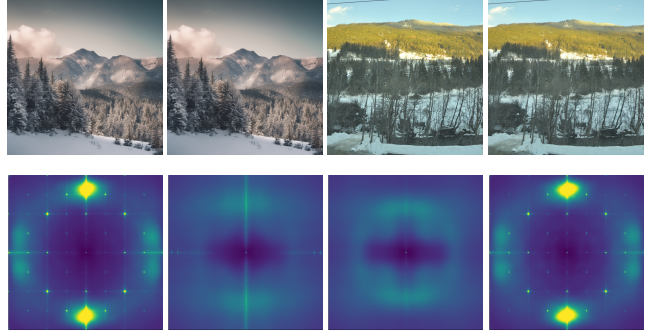


Figure 5. Top (from left to right): a high resolution synthetic image generated by Stable Diffusion XL [58] and its  $4 \times$  decimated version; a real image and the corresponding image obtained at the output of Stable Diffusion [62] used as an autoencoder. Bottom: Fourier spectra of the noise residuals for images shown on the top. A suitable decimation removes Fourier peaks in synthetic images, while passing a real image through an autoencoder creates new peaks.

coder. Therefore, the output (Fig. 5 right) is visually identical to the input but its Fourier spectrum now shows strong peaks. Even so, the CLIP-based detector is not affected by the presence of such traces and the TNR, 97%, is almost the same as with unprocessed images. We find this last experiment to be particularly relevant. In fact, it is very important to take into account malicious operations that can be carried out with the aim of reducing the credibility of current forensic detectors. Of course, several forms of attack can be applied, but this one seems to be especially simple and disruptive, such to easily fool detectors that rely exclusively on low-level traces. Based on this experiment, it seems that the proposed CLIP-based detector looks for different types of traces. Therefore, besides its stand-alone performance, it could be used to complement and enhance the performance of other detectors. A larger set of experiments can be found in the supplementary.

## 5. Comparison with the state-of-the-art

In this Section we perform an extensive comparison with SoTA methods in different scenarios. For our approach we show four variants: trained on 1k real and 1k fake images; 10k real and 10k fake images; trained on 1k and 1k fake images but including compressed/resized images (1k+) and trained on 10k and 10k fake images but including compressed/resized images (10k+). In our analysis we only include SoTA techniques with code and/or pre-trained models publicly available on-line in order to ensure a fair comparison. We considered the following approaches:

- (a) **Wang et al. [71]** is a CNN detector based on ResNet50 and represents a reference in the research community. This work also introduced the large dataset

Method	real/synth. training	size (k)	GAN family					Diffusion family							AVG		
			Pro GAN	Style GAN2	Style GAN3	Style GANT	Giga GAN	Score SDE	ADM	GLIDE	Latent Diff.	Stable Diff.	DeepFl. IF	Ediff-I		DiT	SDXL
Wang et al.	LSUN / ProGAN	360 / 360	100.	96.5	89.0	98.9	66.6	32.9	64.3	48.5	59.2	41.5	78.0	64.9	58.6	54.3	68.1
PatchFor.	CelebA,FF / various	84 / 272	92.3	84.5	87.9	91.2	64.7	83.3	74.8	96.2	78.1	62.4	62.7	78.7	83.1	68.4	79.2
Grag. et al.	LSUN / ProGAN	360 / 360	100.	99.8	<b>98.3</b>	98.8	82.8	92.1	74.7	62.8	91.9	52.5	69.9	69.6	65.3	58.0	79.8
Liu et al.	LSUN / ProGAN	360 / 360	100.	<b>99.8</b>	97.8	98.5	<b>98.2</b>	<b>95.4</b>	82.5	76.5	<b>97.6</b>	77.4	72.2	98.7	88.0	31.1	86.7
Corvi et al.	COCO,LSUN / Latent	180 / 180	79.4	73.7	38.4	97.1	39.9	65.0	80.7	91.9	100.	<b>99.7</b>	<b>99.9</b>	85.7	<b>100.</b>	<b>100.</b>	82.2
LGrad	LSUN / ProGAN	72 / 72	100.	91.2	87.3	81.8	82.2	80.6	76.9	66.1	81.1	61.5	68.8	74.1	56.2	57.2	76.1
Ojha et al.	LSUN / ProGAN	360 / 360	100.	93.9	90.9	98.2	96.0	58.4	<b>86.7</b>	80.8	85.7	89.5	92.9	80.6	77.8	85.1	86.9
DIRE-1	LSUN-Bed / ADM	40 / 40	50.6	56.9	49.3	99.9	74.1	44.3	75.7	71.4	68.7	39.4	98.9	99.1	99.6	47.1	69.7
DIRE-2	LSUN-Bed / St.GAN	40 / 40	54.2	52.5	44.3	99.6	76.0	41.0	70.1	70.1	69.3	46.9	97.0	98.2	98.3	42.8	68.6
Ours 1k	COCO / Latent	1 / 1	98.7	89.8	91.9	100.	81.2	89.4	80.3	<b>99.9</b>	94.0	87.4	96.8	98.7	93.9	89.2	92.2
Ours 1k+	COCO / Latent	1 / 1	89.2	79.7	83.2	99.7	74.2	84.0	74.9	99.6	82.0	89.5	97.8	99.2	91.8	90.3	88.2
Ours 10k	COCO / Latent	10 / 10	<b>99.8</b>	92.5	92.7	<b>100.</b>	84.4	88.0	83.2	99.9	96.2	91.8	97.6	99.2	95.2	88.8	<b>93.5</b>
Ours 10k+	COCO / Latent	10 / 10	87.1	81.8	81.9	99.8	73.5	85.7	79.1	99.3	82.5	90.6	98.4	<b>99.7</b>	93.2	90.8	88.8

Table 3. **Comparison with SOTA methods in terms of AUC.** For our approach we show four variants: trained on 1k real and 1k fake images; 10k real and 10k fake images; trained on 1k and 1k fake images but including compressed/resized images (1k+) and trained on 10k and 10k fake images but including compressed/resized images (10k+). Results obtained on the very same dataset used for training are in light gray, while entries in bold underline the best OOD performance for each dataset. We also report the mean AUC by averaging the AUC scores over all datasets.

Method	real/synth. training	size (k)	GAN family					Diffusion family							AVG		
			Pro GAN	Style GAN2	Style GAN3	Style GANT	Giga GAN	Score SDE	ADM	GLIDE	Latent Diff.	Stable Diff.	DeepFl. IF	Ediff-I		DiT	SDXL
Wang et al.	LSUN / ProGAN	360 / 360	100.	69.2	56.2	71.5	52.8	50.4	50.3	50.7	51.3	50.1	50.0	50.4	50.1	49.8	57.3
PatchFor.	CelebA,FF / various	84 / 272	64.8	50.9	50.1	51.1	51.3	50.0	50.3	50.5	51.3	50.2	50.0	50.0	51.2	50.0	51.5
Grag. et al.	LSUN / ProGAN	360 / 360	100.	<b>96.6</b>	<b>92.6</b>	91.9	69.8	83.8	54.5	56.8	67.5	48.9	48.9	52.1	49.2	51.4	68.9
Liu et al.	LSUN / ProGAN	360 / 360	100.	96.2	78.6	89.4	<b>93.3</b>	<b>89.2</b>	67.2	73.2	<b>84.3</b>	65.3	50.5	92.0	64.3	39.6	77.4
Corvi et al.	COCO,LSUN / Latent	180 / 180	50.0	50.7	50.0	52.0	57.7	50.0	54.5	57.3	99.8	<b>99.7</b>	64.3	50.9	<b>99.8</b>	<b>99.7</b>	66.9
LGrad	LSUN / ProGAN	72 / 72	100.	77.2	62.3	68.5	74.7	60.3	61.2	55.4	69.3	61.5	60.9	62.6	53.2	58.7	66.1
Ojha et al.	LSUN / ProGAN	360 / 360	99.9	77.3	82.4	87.1	81.2	57.1	60.9	57.1	68.1	72.6	65.7	66.0	55.4	68.0	71.3
DIRE-1	LSUN-Bed / ADM	40 / 40	51.4	50.8	50.0	96.5	73.1	50.0	73.2	73.2	73.3	49.7	<b>95.3</b>	<b>95.6</b>	94.9	49.9	69.8
DIRE-2	LSUN-Bed / St.GAN	40 / 40	51.4	50.7	50.0	82.0	66.6	50.0	65.9	65.9	66.4	49.6	80.7	81.5	82.2	49.6	63.7
Ours 1k	COCO / Latent	1 / 1	69.7	72.9	82.0	<b>98.9</b>	69.0	76.6	71.2	<b>97.8</b>	86.9	70.9	63.2	80.3	81.0	60.2	77.2
Ours 1k+	COCO / Latent	1 / 1	68.4	70.3	73.5	96.2	62.9	72.8	65.8	94.7	74.5	77.1	81.6	91.9	78.0	75.2	77.4
Ours 10k	COCO / Latent	10 / 10	<b>90.1</b>	83.0	84.0	98.7	66.5	75.6	<b>72.3</b>	93.7	89.9	72.9	59.5	78.8	76.8	54.4	<b>78.3</b>
Ours 10k+	COCO / Latent	10 / 10	73.8	72.3	71.4	95.0	60.8	75.6	68.2	90.5	74.4	77.3	81.7	92.4	77.4	70.0	77.2

Table 4. **Comparison with SOTA methods in terms of Accuracy, fixed 0.5 threshold.** Results obtained on the very same dataset used for training are in light gray, while entries in bold underline the best OOD performance for each dataset. We also report the mean Accuracy by averaging the Accuracy scores over all datasets.

- (LSUN/ProGAN) extensively adopted for model training in subsequent works.
- Grag et al. [33]** proposes a simple modification to the ResNet50 architecture which allows to better preserve low-level forensic traces and is trained on the same dataset introduced in [71].
  - PatchForensics [9]** develops a fully-convolutional classifier based on local patches with limited receptive fields over an XceptionNet backbone.
  - Liu et al. [47]** is a detector that exploits the inconsistency between real and fake images in the representations of the learned noise patterns. This spatial information is combined with frequency information to improve the classification.
  - LGrad [69]** works on the gradients extracted through a pre-trained CNN model in order to filter out the content of the image and transform a data-dependent problem into a transformation-model dependent problem.
  - Corvi et al. [14]** performs strong augmentation to gain robustness and increase generalization and is trained on a large dataset of latent diffusion models.
  - Ojha et al. [56]** uses CLIP-based features and performs detection using the CLIP feature space. Both nearest neighbor and linear probing are tested, even if the latter gives better performance.
  - DIRE [72]** is based on the idea that synthetic images can be reconstructed better than real images by a pre-trained model. To this end it is proposed to train a ResNet-50 in two different ways, using ADM images (DIRE 1) and StyleGAN images (DIRE 2), respectively.
- Comparison over GAN- and DM-based generators.** In Tab. 3 and Tab. 4 we show results in terms of AUC and Accuracy, respectively, over 14 GAN-based and DM-based

generators proposed in the scientific literature and perfectly known. For each method, results obtained on the very same dataset used for training are in light gray, to signal an ID scenario, of little interest for our analysis. Entries in bold, instead, underline the best OOD performance for each dataset. Focusing on AUC data, Tab. 3, we observe that methods trained on a GAN dataset work generally well on other dataset of the same family, and much worse on DM datasets. Then, the roles switch for methods trained on DM datasets. This is nothing new, as generators of the two families share architectural details that leave similar traces on the generated images. No SoTA method works uniformly well on all datasets. On the contrary, the proposed lightweight CLIP-based detector provides a uniformly good performance, and the version with 10k+10k reference images without augmentation outperforms the best competitor (notably, again a CLIP-based method) by +6.6%, obtaining an average AUC well above 93.5% a truly impressive accomplishment.

In terms of Accuracy, Tab. 4, performance lowers significantly, and in some cases dramatically. The proposed CLIP-based detectors keep providing the best performance, generally much better than SoTA methods, except for Liu’s method that performs almost at the same level.

**Comparison over commercial tools.** However, the performance of Liu’s method, as well as that of several other methods, drops catastrophically when considering the Commercial Tools (DALL-E2, DALL-E3, Midjourney, FireFly) both in terms of AUC and Accuracy, see Tab. 5. Needless to say, this is the most realistic and interesting scenario, often with images of unknown origin and no prior information on the possible generation process. In this situation, most methods provide unreliable decisions. Corvi’s method works surprisingly well on some datasets, maybe generated by diffusion models similar to Latent. However, only the proposed CLIP-based approach provides a stable good performance in all cases. Note that, now, the versions with resized and recompressed images in the reference set perform significantly better than those without augmentation.

**Robustness to perturbations.** The trend observed over unknown models is further accentuated when images are subject to some post-processing, Tab. 6. These impairments tend to wash out forensic traces, to the point that most SoTA methods become basically useless with coin-tossing performance, especially on the unknown commercial models. Again, the CLIP-based detectors provide a more than decent performance, further supporting our conjecture on the high-level nature of the forensic traces they rely upon.

## 6. Discussion

In this work, we have shown a series of good features of CLIP that can help detecting real from synthetic content. Through an extensive experimental analysis we found that:

Method	Commercial tools				Average AUC/Acc
	DALL-E2 AUC/Acc	DALL-E3 AUC/Acc	Midjourney AUC/Acc	FireFly AUC/Acc	
Wang et al.	64.8 / 50.2	10.9 / 49.4	40.2 / 49.5	84.8 / 50.3	50.2 / 49.8
PatchFor.	41.9 / 50.0	52.7 / 50.0	57.8 / 50.0	49.4 / 50.0	50.5 / 50.0
Grag. et al.	58.3 / 49.2	2.4 / 36.9	43.1 / 40.5	63.5 / 47.5	41.8 / 43.6
Liu et al.	70.4 / 66.4	0.2 / 30.8	40.7 / 43.3	11.8 / 31.0	30.8 / 42.9
Corvi et al.	69.4 / 50.1	60.8 / 50.0	<b>100. / 100.</b>	<b>98.0 / 51.1</b>	82.1 / 62.8
LGrad	58.6 / 55.5	37.9 / 47.8	56.3 / 57.9	40.6 / 47.5	48.3 / 52.1
Ojha et al.	<b>95.2 / 83.5</b>	36.4 / 47.3	66.2 / 52.4	97.5 / 89.9	73.8 / 68.3
DIRE-1	44.7 / 50.0	47.6 / 50.0	51.0 / 49.7	57.4 / 49.9	50.2 / 49.9
DIRE-2	41.0 / 49.9	49.6 / 50.0	47.8 / 49.8	43.0 / 49.8	45.3 / 49.9
Ours 1k	89.1 / 62.2	77.6 / 53.4	74.3 / 53.2	77.1 / 52.1	79.5 / 55.2
Ours 1k+	83.9 / 68.2	<b>94.8 / 83.1</b>	79.7 / 64.7	86.0 / <b>68.4</b>	86.1 / <b>71.1</b>
Ours 10k	88.8 / 57.8	82.9 / 51.1	75.4 / 51.2	79.9 / 50.9	81.7 / 52.8
Ours 10k+	84.5 / 63.9	94.4 / 76.6	83.8 / 62.7	87.6 / 64.5	<b>87.6 / 67.0</b>

Table 5. **AUC/Accuracy on Commercial Tools.** We show AUC and Accuracy on very recent synthetic generators: DALL-E2, DALL-E3, Midjourney v5 and Firefly.

Method	Families of Generators			Average AUC/Acc
	GAN AUC/Acc	Diffusion AUC/Acc	Comm. Tools AUC/Acc	
Wang et al.	78.9 / 62.1	59.3 / 50.4	44.1 / 49.9	60.8 / 54.1
PatchFor.	54.3 / 50.0	64.8 / 50.3	62.9 / 50.1	60.7 / 50.1
Grag. et al.	<b>89.2 / 68.5</b>	67.9 / 50.8	47.3 / 50.0	68.1 / 56.4
Liu et al.	54.7 / 51.6	56.3 / 51.1	53.0 / 50.7	54.6 / 51.1
Corvi et al.	66.7 / 54.1	76.1 / 62.1	52.1 / 50.1	65.0 / 55.4
LGrad	51.2 / 51.0	48.0 / 50.5	49.4 / 50.4	49.5 / 50.7
Ojha et al.	86.9 / <b>74.9</b>	73.7 / 59.8	49.6 / 50.6	70.1 / 61.8
DIRE-1	48.9 / 50.3	51.0 / 50.5	50.1 / 49.9	50.0 / 50.2
DIRE-2	49.1 / 50.0	52.3 / 52.5	45.3 / 49.9	48.9 / 50.8
Ours 1k	76.4 / 68.7	81.2 / 71.4	74.3 / 61.9	77.3 / 67.3
Ours 1k+	75.3 / 67.8	87.8 / <b>77.6</b>	<b>84.2 / 66.0</b>	82.4 / <b>70.4</b>
Ours 10k	76.8 / 60.7	82.7 / 59.6	73.8 / 50.5	77.8 / 56.9
Ours 10k+	78.2 / 67.9	<b>88.7 / 77.0</b>	83.0 / 65.6	<b>83.3 / 70.2</b>

Table 6. **AUC/Accuracy in the presence of post-processing.** All the images have been randomly cropped, resized and compressed to simulate a realistic scenario over the web.

- CLIP features support a much higher generalization ability than what had been discovered so far. By leveraging just a few examples, not even belonging to the generator under test, a simple CLIP-based detector achieves top performance on a large variety of generators and in the most challenging conditions.
- Maximizing the diversity of reference CLIP features impacts positively on performance, even when a relatively large number of examples is considered.
- It is well known that CLIP descriptive power descends from its huge pre-training set. Further increasing this set keeps boosting the performance, up to 10%.
- Experimental evidence seems to show that CLIP features, even when tuned to forensic applications, are mostly independent from low-level forensic traces. This opens the way to interesting developments. On one hand, one can gain immunity to possible malicious attacks working on low-level artifacts. On the other hand, there is room for

further performance improvement by suitable fusion with classic detectors.

Overall, the present study provides a number of interesting insights but leaves much room for future work. We believe that new and better forensic methods can be proposed on top of CLIP. One major area of study can be to develop few-shot methods that adapt the detector on the fly to the situation of interest. Future work should also consider interpretability, to begin with understanding which forensic features the detector exploits to make its decisions.

**Acknowledgment.** We gratefully acknowledge the support of this research by a TUM-IAS Hans Fischer Senior Fellowship, a TUM-IAS Rudolf Mößbauer Fellowship and a Google Gift. This material is also based on research sponsored by the Defense Advanced Research Projects Agency (DARPA) and the Air Force Research Laboratory (AFRL) under agreement number FA8750-20-2-1004. The U.S. Government is authorized to reproduce and distribute reprints for Governmental purposes notwithstanding any copyright notation thereon. The views and conclusions contained herein are those of the authors and should not be interpreted as necessarily representing the official policies or endorsements, either expressed or implied, of DARPA or the U.S. Government. In addition, this work has received funding by the European Union under the Horizon Europe vera.ai project, Grant Agreement number 101070093. It is also supported by the PREMIER project, funded by the Italian Ministry of Education, University, and Research within the PRIN 2017 program. Finally, we want to thank Koki Nagano for useful discussions, and Tero Karras, Yogesh Balaji, Ming-Yu Liu for sharing data for StyleGAN-T and eDiff-I experiments.

## Supplemental Material

In this appendix, we report additional ablation studies (Sec. A) and robustness analysis (Sec. B). We also enlarge our initial dataset with additional synthetic generators and carry out further experiments on generalization (Sec. C). Furthermore, we conduct more experiments on the ability of our approach and SoTA methods to deal with possible attacks from malicious users (Sec. D). Finally, we show some experiments carried out on social networks in a few-shot scenario (Sec. E).

### A. Additional ablation study

In Section 4 of the paper we describe the CLIP-based detection procedure used in all experiments. Two important design choices outlined in the paper are that *i*) we extract features from the next to last layer of the CLIP ViT L/14 architecture; and *ii*) we use a SVM classifier, designed based

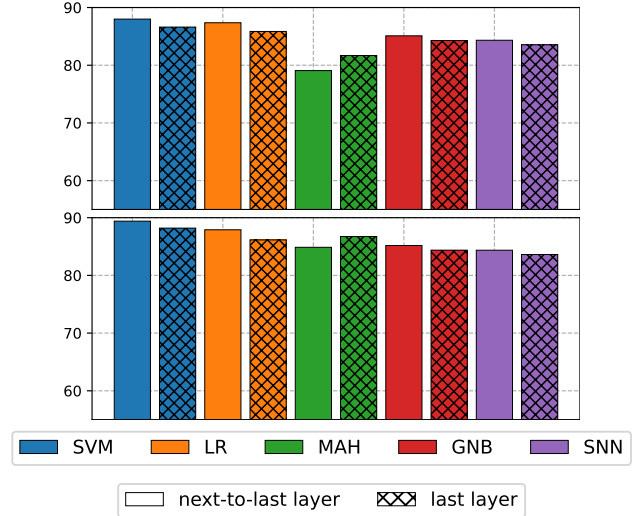


Figure 6. Average AUC for our approach considering different classifiers and different features on the original dataset. Top: 1k images, Bottom: 10k images.

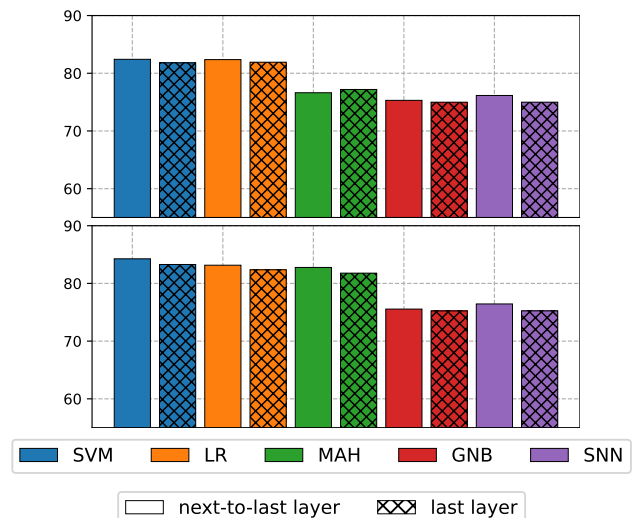


Figure 7. Average AUC for our approach considering different classifiers and different features on the dataset after random compression and resizing. Top: 1k images, Bottom: 10k images.

on a limited set of reference features. Here we test some alternative solutions, that is:

- extracting features from the last layer of the architecture;
- using other classifiers: Logistic Regression (LR), Mahalanobis distance (MAH), Gaussian Naive Bayes classifier (GNB), Soft voting k-Nearest Neighbor (SNN) [54].

In Figures 6 and 7, we show the results in terms of average AUC over the dataset described in Section 3 (main paper) using both original images and images impaired by common post-processed steps such as recompression and resizing. For all detectors, we consider the versions 1k and 10k

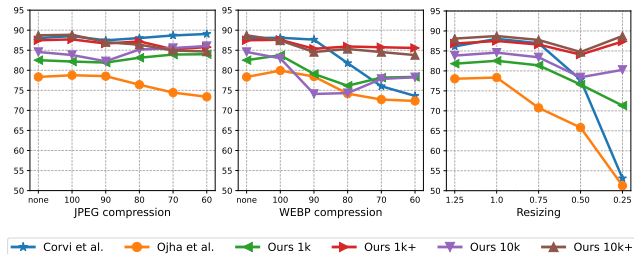


Figure 8. Robustness analysis in terms of AUC carried out on the Stable Diff. 2, SDXL, DALL-E 3, DALL-E 2, Midjourney, and Firefly generation models of the SynthBuster dataset [4].

(1000 and 10000 reference images, respectively).

In all cases, the SVM classifier seems to ensure the best performance, followed closely by the Logistic Regression, while the other classifiers provide a less consistent performance. Using features from the next-to-last layer is almost always preferable to using features from the last layer, and this happens always with the SVM classifier. These results motivated our design choices.

## B. Additional robustness analysis

In Section 5 of the paper, in Tab. 6, we provide some results on the robustness of SoTA and proposed methods in the presence of image impairments. Due to lack of space, however, we show only some very synthetic results, averaged on generic post-processed images. Here, we analyze robustness in more detail as a function of the JPEG Quality Factor, which ranges from 100 to 60, and the resizing scale, which ranges from 125% to 25%. In addition, we consider also another compression method, WEBP, which is gaining popularity on social networks and has been rarely been used for augmentation. Images are from the SynthBuster dataset [4], generated by Stable Diffusion 2, SDXL, DALL-E 2, DALL-E 3, Midjourney, and Firefly. We show results (AUC) only for the most competitive (in terms of robustness) SoTA methods, Corvi and Ojha. For our method we consider again four variants similarly to the main paper: the versions using 1k or 10k real and fake reference images, and the corresponding versions, 1k+ and 10k+, where data have been augmented with randomly compressed/resized images, while keeping constant the total number of images.

Ojha suffers some performance losses, up to 10 points, in the presence of compression, be it JPEG or WEBP, and a much more rapid decline with resizing, to the point of becoming useless in the presence of a 25% rescaling. Corvi was trained with strong augmentation and, in fact, is not affected at all by JPEG compression, while it presents acceptable losses with strong WEBP compression (not seen in training), and strong resizing. The most remarkable outcome of this experiment, however, is the impressive robustness of the CLIP-based detectors. Both the 1k+ and 10k+

Generator	modality	LSUN [76]	FFHQ [41]	ImageNet [18]	COCO [46]	Resolution
BigGAN [7]	c			✓		256 <sup>2</sup> , 512 <sup>2</sup>
EG3D [10]	u		✓			512 <sup>2</sup>
Diff.ProjecteGAN [73]	u	✓				256 <sup>2</sup>
GALIP [70]	t				✓	224 <sup>2</sup>
Taming Transf. [27]	u,c		✓	✓		256 <sup>2</sup>
DALL-E mini [17]	t				✓	256 <sup>2</sup>
DDPM [34]	u		✓			256 <sup>2</sup>
Deepfloyd-IF II stage [44]	t				✓	256 <sup>2</sup>

Table 7. Image generators used in our experiments: GAN-based, VQ-GAN-based and DM-based. The generation modalities, unconditional (u), conditional (c), and text-to-image (t), is reported in the second column. The last column reports the resolution of the images in the dataset.

versions, the ones with augmentation, are basically insensitive to compression, no matter JPEG or WEBP, and resizing. The versions without augmentation suffer some loss of performance but not nearly as dramatic as for the reference methods, and remain effective in all conditions.

## C. Further generalization results

In this Section we extend our generalization analysis to additional data. In the main paper we included 6,000 real images and 18,000 fake images from 18 models, now we consider 8 more generators with 8,000 additional synthetic images for our test set (Tab. 7). The StyleGAN-T [63], eDiff-I [3], and GigaGAN [39] images are provided by the authors of the original papers. Instead, we ourselves generated images for Score-SDE [68], Stable Diff. [62], DiT [57], Deepfloyd-IF [44], Diff.ProjecteGAN [73], GALIP [70], and DDPM [34] using the pre-trained models available online. The other generated images come from three public datasets [4, 14, 71]. To avoid possible biases, performance metrics are evaluated using for each fake dataset images drawn from the real dataset used in training, indicated in the central columns of Table 1 of main paper and Table 7 of this supplemental.

In Tab. 8 we show the results in terms of AUC and Accuracy on such data for the four version of the proposed CLIP-based detector and for the SoTA methods described in the main paper (Section 5): Wang et al. [71], Grag et al. [33], PatchForensics [9], Liu et al. [47], LGrad [69], Corvi et al. [14], Ojha et al. [56], DIRE [72].

We can observe that SoTA methods present a larger variability in terms of performance, with very good results on some generators and very bad on others. Instead, our method can provide consistently good performance over all the data both in terms of AUC and Accuracy, with an aver-

AUC/Acc Method	BigGAN	EG3D	Diff. Proj. GAN	GALIP	Taming Transf.	DALL-E Mini	DDPM	Deepfloyd-IF II stage	AVG
[71] Wang et al.	92.7 / 66.1	94.4 / 59.2	89.8 / 52.1	89.7 / 57.4	54.3 / 51.7	62.5 / 51.8	31.6 / 50.1	43.1 / 50.1	69.8 / 54.8
[9] PatchFor.	85.5 / 52.5	69.8 / 50.0	92.6 / 61.7	98.2 / 73.4	71.2 / 51.0	83.8 / 51.4	98.4 / 50.2	83.4 / 50.0	85.4 / 55.0
[33] Grag. et al.	98.7 / 94.2	98.9 / <b>93.8</b>	<b>100.</b> / 72.5	96.2 / 79.5	90.3 / 76.4	83.4 / 62.5	49.7 / 45.1	71.2 / 61.3	86.0 / 73.2
[47] Liu et al.	94.7 / 81.3	<b>99.0</b> / 86.3	99.5 / 84.9	94.3 / 78.4	95.4 / 78.9	98.4 / 88.1	22.8 / 49.6	97.4 / 86.8	87.7 / 79.3
[14] Corvi et al.	83.4 / 51.8	25.2 / 50.0	96.6 / 71.2	87.7 / 50.9	99.3 / 89.5	99.7 / 83.8	<b>100.</b> / <b>90.3</b>	68.5 / 50.8	82.5 / 67.3
[69] LGrad	77.2 / 69.0	68.8 / 59.8	99.5 / <b>90.1</b>	56.7 / 55.1	74.1 / 64.5	67.3 / 59.9	9.8 / 16.4	75.0 / 62.5	66.1 / 59.7
[56] Ojha et al.	99.6 / <b>96.4</b>	92.6 / 82.5	97.4 / 75.2	98.6 / 89.9	94.1 / 84.8	97.1 / 84.9	77.7 / 68.2	60.8 / 50.0	89.7 / 79.0
[72] DIRE-1	<b>99.8</b> / 95.3	50.1 / 50.0	49.8 / 51.6	100. / 96.7	73.1 / 72.4	99.7 / 96.5	23.1 / 50.0	99.4 / <b>95.8</b>	74.4 / 76.0
[72] DIRE-2	98.6 / 82.4	46.1 / 50.0	50.2 / 51.4	99.3 / 81.8	77.0 / 66.2	98.7 / 81.8	14.0 / 49.8	95.6 / 80.5	72.4 / 68.0
Ours 1k	96.7 / 85.2	86.3 / 73.8	99.3 / 69.7	100. / 99.7	99.3 / 94.3	100. / 98.9	94.7 / 86.0	99.7 / 90.6	97.0 / 87.3
Ours 1k+	90.9 / 77.4	75.5 / 64.7	89.4 / 68.4	99.9 / 98.2	93.4 / 82.3	99.6 / 94.0	94.6 / 87.7	99.7 / 95.1	92.9 / 83.5
Ours 10k	98.2 / 85.9	90.8 / 81.4	99.8 / 90.1	<b>100.</b> / <b>99.9</b>	<b>99.6</b> / <b>94.3</b>	<b>100.</b> / <b>99.1</b>	94.9 / 88.3	<b>99.8</b> / 88.1	<b>97.9</b> / <b>90.9</b>
Ours 10k+	91.7 / 75.0	80.7 / 72.5	88.9 / 74.6	100. / 97.8	92.5 / 77.2	99.8 / 93.5	95.9 / 79.5	99.8 / 92.8	93.7 / 82.8

Table 8. **Comparison with SOTA methods on additional data.** The results are in terms of AUC/Accuracy. The entries in bold underline the best performance for each dataset. For our approach we show four variants: trained on 1k real and 1k fake images; 10k real and 10k fake images; trained on 1k and 1k fake images but including compressed/resized images (1k+) and trained on 10k and 10k fake images but including compressed/resized images (10k+).

AUC/Acc Method	BigGAN	EG3D	Diff. Proj. GAN	GALIP	Taming Transf.	DALL-E Mini	DDPM	Deepfloyd-IF II stage	AVG
[71] Wang et al.	82.5 / 55.5	84.7 / 52.2	80.8 / 53.2	92.2 / 59.2	66.2 / 50.6	66.7 / 50.5	69.6 / 50.2	47.9 / 49.9	73.8 / 52.7
[9] PatchFor.	58.7 / 50.3	60.3 / 50.0	55.6 / 50.0	72.3 / 50.3	50.4 / 50.1	71.0 / 50.1	82.9 / 51.0	69.7 / 50.0	65.1 / 50.2
[33] Grag. et al.	<b>97.6</b> / 74.4	<b>92.7</b> / 56.5	<b>99.2</b> / 65.6	99.1 / 79.8	83.6 / 53.3	89.6 / 54.0	74.5 / 49.4	54.3 / 50.0	86.3 / 60.4
[47] Liu et al.	57.7 / 52.0	51.6 / 50.4	62.9 / 54.1	65.2 / 52.3	49.2 / 50.2	49.1 / 50.7	58.3 / 49.1	64.4 / 52.0	57.3 / 51.4
[14] Corvi et al.	77.3 / 53.0	64.5 / 59.7	93.3 / 59.8	87.4 / 51.5	<b>94.4</b> / 76.7	97.4 / 74.8	74.7 / 59.6	70.4 / 50.9	82.4 / 60.7
[69] LGrad	53.5 / 51.6	53.2 / 51.1	56.9 / 51.1	57.0 / 50.3	51.3 / 51.1	41.7 / 49.1	56.0 / 49.7	38.7 / 48.8	51.0 / 50.4
[56] Ojha et al.	94.8 / <b>84.9</b>	79.3 / 61.5	84.7 / <b>68.5</b>	95.7 / 84.5	92.9 / <b>81.8</b>	89.1 / 72.8	90.8 / 79.1	59.1 / 49.5	85.8 / 72.8
[72] DIRE-1	47.2 / 49.5	35.2 / 49.3	35.2 / 49.6	47.4 / 50.6	47.3 / 49.7	54.6 / 51.1	38.5 / 49.4	64.6 / 53.2	46.2 / 50.3
[72] DIRE-2	44.6 / 47.0	33.6 / 47.1	37.5 / 44.9	46.2 / 47.2	43.3 / 46.8	53.1 / 50.0	42.2 / 47.5	66.3 / 59.3	45.9 / 48.7
Ours 1k	84.0 / 74.8	64.4 / 59.5	75.3 / 68.3	98.5 / 93.0	85.3 / 75.0	96.5 / 89.0	76.7 / 66.6	90.6 / 80.1	83.9 / 75.8
Ours 1k+	88.9 / 78.2	60.0 / 54.6	70.5 / 60.9	99.8 / 98.3	86.5 / 77.3	98.9 / 93.6	<b>96.1</b> / <b>84.7</b>	99.4 / 96.2	87.5 / <b>80.5</b>
Ours 10k	84.4 / 59.1	70.9 / <b>63.3</b>	68.8 / 55.6	99.2 / 79.7	85.7 / 67.7	97.5 / 68.7	64.6 / 57.0	95.1 / 62.2	83.3 / 64.1
Ours 10k+	91.3 / 79.4	68.7 / 59.7	68.7 / 61.7	<b>99.9</b> / <b>99.0</b>	86.2 / 71.2	<b>99.4</b> / <b>93.6</b>	92.7 / 62.4	<b>99.8</b> / <b>97.8</b>	<b>88.3</b> / 78.1

Table 9. **Comparison with SOTA methods on additional data in the presence of post-processing.** The results are in terms of AUC/Accuracy. The entries in bold underline the best performance for each dataset.

age gain over the best reference of around 8% in terms of AUC and 11% in terms of Accuracy. This difference is even more noticeable on data that have undergone random compression and resizing (Tab. 9). In fact, for most of the competitors there is a dramatic performance loss, sometimes to a random guess level. Some other methods, such as, Ohja et al., preserve a good performance and the same happens for ours. Of course, in this more challenging scenario our best variant is the one that includes some form of augmentation in the reference data but even the variant trained on the original data provides satisfying results.

## D. Attack scenario

In this section, we conduct some additional experiments on a specific attack scenario, where a malicious user takes real images and passes them through the autoencoder of a specific generative model. The objective is to insert the low-level traces typical of synthetic architectures in real images in order to fool forensic detectors and make everything ap-

pear as synthetic. To this end, we took 1000 real images from the RAISE dataset [16] and passed them through the autoencoders of three different versions of diffusion models: Stable Diffusion 1.4, Stable Diffusion 2.0 [62] and Stable Diffusion XL [58]. In Fig. 9 we show that such process insert exactly the same forensic clues in the real images and they appear indistinguishable from the generated ones, without altering their visual appearance (see Fig. 5 of the main paper).

In Table 10 we report results in terms of accuracy before and after the attack for our method and the best competitors. Before the attack, the detector must discriminate between real and generated images while, after the attack, it must discriminate between laundered real images and generated ones. We notice that before the attack the method proposed by Corvi et al. can achieve almost perfect results. However, it is very sensitive to the insertion of low-level traces and provides totally wrong results on the attacked data. For Ojha et al the performance also worsen, with an average 7%

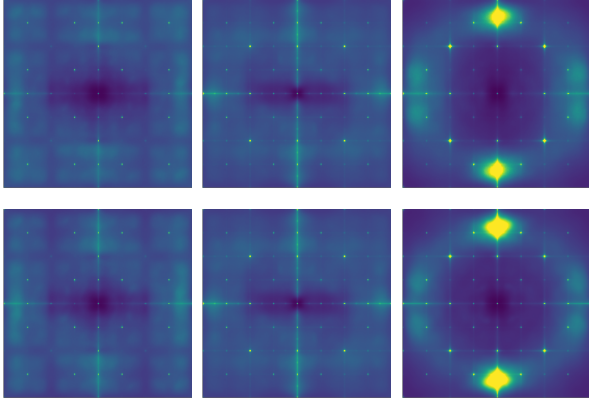


Figure 9. Top (from left to right): Fourier spectra of the noise residuals for synthetic images generated with Stable Diffusion 1.4, Stable Diffusion 2.0 and Stable Diffusion XL. Bottom: Fourier spectra of the noise residuals for the real images that passed through the corresponding autoencoder of the synthetic generators. We can observe that this operation has inserted in the real images exactly the same artifacts present in the synthetic ones.

Accuracy	before the attack			after the attack		
	St.Diff. 1.4	St.Diff. 2.0	SDXL	St.Diff. 1.4	St.Diff. 2.0	SDXL
Corvi et al.	100.	99.2	99.7	50.0	49.2	53.7
Ojha et al.	69.9	75.6	68.0	59.0	69.0	64.5
Ours 1k	63.6	64.3	60.2	63.6	63.8	59.2
Ours 1k+	76.8	77.0	75.2	77.0	75.5	72.6
Ours 10k	65.8	60.5	54.4	65.9	60.2	54.0
Ours 10k+	78.8	72.8	70.0	79.1	71.5	68.7

Table 10. Results in terms of Accuracy before and after the laundering attack on real images. Before the attack all methods achieve a very good performance. After the attack the performance of our method is almost unchanged, while significant losses are observed for the best reference methods, especially for Corvi et al. that goes from perfect detection to random guess.

loss. Instead, for our method the Accuracy is almost unaffected by the attack, with an average loss below 1.3%.

Based on these results, it appears that the proposed CLIP-based detector does not rely on the same low-level traces exploited by most of the current detectors. This ensures higher robustness to common attacks and opens the way to the use of suitable fusion strategies. However, there is much room for further analysis, to begin with identifying which traces our detector is actually exploiting.

## E. Few-shot analysis in the wild

In this section we present an experiment in a few-shot scenario. The idea is to explore the ability of our detector to work with very limited data and adapt to a situation where



Figure 10. Some examples of images downloaded from the social network Twitter. From left to right: a real image, synthetic images from DALL-E 3 [6], Firefly [30], Midjourney [52].

AUC/Acc	Twitter			Average
	DALL-E3	Midjourney	FireFly	
Ours 1k	71.9 / 51.1	70.3 / 54.0	77.4 / 52.4	73.2 / 52.5
Ours 1k+	83.6 / 72.3	75.5 / 67.3	89.6 / 80.5	82.9 / 73.4
Ours 10k	68.2 / 50.5	72.0 / 51.5	70.7 / 51.5	70.3 / 51.2
Ours 10k+	67.0 / 60.0	78.3 / 71.0	74.3 / 68.5	73.2 / 66.5
Ours Few-Shot	<b>97.7 / 90.6</b>	<b>91.9 / 82.5</b>	<b>96.6 / 88.4</b>	<b>95.4 / 87.2</b>

Table 11. We show results in a few-shot experiment, where we suppose to know in advance 10+10 real/fake images from a specific generator and compare them with our basic approach trained on a larger set of real/fake images from misaligned data. As can be seen, even with just 10 images it is possible to adapt the model and obtain a large improvement.

only a few real and synthetic examples are available. We downloaded real and synthetic images from Twitter and considered three different generators DALL-E 3, Midjourney and Firefly (some examples can be seen in Fig. 10). To understand which generator was used to create a specific image, we relied on tags and annotations present on the social network.

In our few-shot scenario, we take 10 real images and 10 generated images as examples from a specific model and test on all the others images (note that we present average results on 1000 runs). Results are reported in Tab. 11 in terms of AUC and Accuracy. The availability of just 10+10 images of the target data provides an impressive performance boost with respect to the same method trained on a larger dataset, but not aligned with the test data (real images come from COCO, synthetic images from Latent diffusion models). It is important to underline that this is a realistic scenario, in which one is called to decide on images generated by a new method and a few sample images are available as a support. We believe that this can represent an interesting direction for the application in the wild or to easily adapt a detector to more challenging situations where some prior information is available.

## References

- [1] Michael Albright and Scott McCloskey. Source Generator Attribution via Inversion. In *CVPR Workshops*, pages 96–103, 2019. 3
- [2] Roberto Amoroso, Davide Morelli, Marcella Cornia,

- Lorenzo Baraldi, Alberto Del Bimbo, and Rita Cucchiara. Parents and Children: Distinguishing Multi-modal DeepFakes from Natural Images. *arXiv preprint arXiv:2304.00500v1*, 2023. 2, 3
- [3] Yogesh Balaji, Seungjun Nah, Xun Huang, Aarash Vahdat, Jiaming Song, Kreis Kreis, Miika Aittala, Timo Aila, Samuli Laine, Bryan Catanzaro, Tero Karras, and Ming-Yu Liu. eDiff-I: Text-to-Image Diffusion Models with an Ensemble of Expert Denoisers. *arXiv preprint arXiv:2211.01324v5*, 2022. 4, 10
- [4] Quentin Bammey. Synthbuster: Towards detection of diffusion model generated images. *IEEE OJSP*, 2023. 4, 10
- [5] Clark Barrett, Brad Boyd, Elie Burzstein, Nicholas Carlini, Brad Chen, Jihye Choi, Amrita Roy Chowdhury, Mihai Christodorescu, Anupam Datta, and Soheil Feizi et al. Identifying and Mitigating the Security Risks of Generative AI. *arXiv preprint arXiv:2308.14840v3*, 2023. 1
- [6] James Betker, Gabriel Goh, Li Jing, Tim Brooks, Jianfeng Wang, Linjie Li, Long Ouyang, Juntang Zhuang, Joyce Lee, Yufei Guo, Wesam Manassra, Prafulla Dhariwal, Casey Chu, and Yunxin Jiao. <https://openai.com/dall-e-3>, 2023. 3, 4, 12
- [7] Andrew Brock, Jeff Donahue, and Karen Simonyan. Large Scale GAN Training for High Fidelity Natural Image Synthesis. In *ICLR*, 2018. 10
- [8] Joao Phillipe Cardenuto, Jing Yang, Rafael Padilha, Renjie Wan, Daniel Moreira, Haoliang Li, Shiqi Wang, Fernanda Andalò, Sébastien Marcel, and Anderson Rocha. The Age of Synthetic Realities: Challenges and Opportunities. *arXiv preprint arXiv:2306.11503v1*, 2023. 1
- [9] Lucy Chai, David Bau, Ser-Nam Lim, and Phillip Isola. What Makes Fake Images Detectable? Understanding Properties that Generalize. In *ECCV*, pages 103–120, 2020. 2, 7, 10, 11
- [10] Eric Ryan Chan, Connor Zhizhen Lin, Matthew Aaron Chan, Koki Nagano, Boxiao Pan, Shalini De Mello, Orazio Gallo, Leonidas Guibas, Jonathan Tremblay, Sameh Khamis, Tero Karras, and Gordon Wetzstein. Efficient geometry-aware 3d generative adversarial networks. In *CVPR*, pages 16123–16133, 2022. 10
- [11] Keshigeyan Chandrasegaran, Ngoc-Trung Tran, and Ngai-Man Cheung. A Closer Look at Fourier Spectrum Discrepancies for CNN-Generated Images Detection. In *CVPR*, pages 7200–7209, 2021. 3
- [12] Keshigeyan Chandrasegaran, Ngoc-Trung Tran, Alexander Binder, and Ngai-Man Cheung. Discovering Transferable Forensic Features for CNN-Generated Images Detection. In *ECCV*, pages 671–689, 2022. 2
- [13] Riccardo Corvi, Davide Cozzolino, Giovanni Poggi, Koki Nagano, and Luisa Verdoliva. Intriguing properties of synthetic images: from generative adversarial networks to diffusion models. In *CVPR Workshops*, pages 973–982, 2023. 1, 3
- [14] Riccardo Corvi, Davide Cozzolino, Giada Zingarini, Giovanni Poggi, Koki Nagano, and Luisa Verdoliva. On the detection of synthetic images generated by diffusion models. In *ICASSP*, pages 1–5, 2023. 2, 3, 7, 10, 11
- [15] Davide Cozzolino, Justus Thies, Andreas Rössler, Christian Riess, Matthias Nießner, and Luisa Verdoliva. Forensic-Transfer: Weakly-supervised domain adaptation for forgery detection. *arXiv preprint arXiv:1812.02510v2*, 2018. 2
- [16] Duc-Tien Dang-Nguyen, Cecilia Pasquini, Valentina Conotter, and Giulia Boato. RAISE: A Raw Images Dataset for Digital Image Forensics. In *ACM MMSys*, page 219–224, 2015. 4, 11
- [17] Boris Dayma, Suraj Patil, Pedro Cuenca, Khalid Saifullah, Tanishq Abraham, Phúc Lê Khắc, Luke Melas, and Ritobrata Ghosh. <https://github.com/borisdayma/dalle-mini>, 2021. 10
- [18] Jia Deng, Wei Dong, Richard Socher, Li-Jia Li, Kai Li, and Li Fei-Fei. ImageNet: A large-scale hierarchical image database. In *CVPR*, pages 248–255, 2009. 4, 10
- [19] Prafulla Dhariwal and Alex Nichol. Diffusion models beat GANs on image synthesis. In *NeurIPS*, pages 8780–8794, 2021. 4
- [20] Chengdong Dong, Ajay Kumar, and Eryun Liu. Think Twice Before Detecting GAN-Generated Fake Images From Their Spectral Domain Imprints. In *CVPR*, pages 7865–7874, 2022. 3
- [21] Mengnan Du, Shiva Pentylala, Yuening Li, and Xia Hu. Towards Generalizable Deepfake Detection with Locality-Aware AutoEncoder. In *CIKM*, page 325–334, 2020. 2
- [22] Ricard Durall, Margret Keuper, and Janis Keuper. Watch Your Up-Convolution: CNN Based Generative Deep Neural Networks Are Failing to Reproduce Spectral Distributions. In *CVPR*, pages 7890–7899, 2020. 1, 3
- [23] Tarik Dzanic, Karan Shah, and Freddie D. Witherden. Fourier spectrum discrepancies in deep network generated images. In *NeurIPS*, pages 3022–3032, 2020. 3
- [24] David C. Epstein, Ishan Jain, Oliver Wang, and Richard Zhang. Online Detection of AI-Generated Images. In *ICCV Workshops*, pages 382–392, 2023. 3
- [25] Ziv Epstein, Aaron Hertzmann, Laura Herman, Robert Mahari, Morgan R. Frank, Matthew Groh, Hope Schroeder, Amy Smith, Memo Akten, and Jessica Fjeld et al. Art and the science of generative AI: A deeper dive. *arXiv preprint arXiv:2306.11503v1*, 2023. 1
- [26] Sepideh Esmaeilpour, Bing Liu, Eric Robertson, and Lei Shu. Zero-shot out-of-distribution detection based on the pretrained model clip. In *AAAI*, pages 6568–6576, 2022. 2
- [27] Patrick Esser, Robin Rombach, and Björn Ommer. Taming transformers for high-resolution image synthesis. In *CVPR*, pages 12873–12883, 2021. 10
- [28] Hany Farid. Lighting (in)consistency of paint by text. *arXiv preprint arXiv:2207.13744v2*, 2022. 2
- [29] Hany Farid. Perspective (in)consistency of paint by text. *arXiv preprint arXiv:2206.14617v1*, 2022. 2
- [30] Adobe Firefly. <https://www.adobe.com/sensei/generative-ai/firefly.html>, 2023. 3, 4, 12
- [31] Joel Frank, Thorsten Eisenhofer, Lea Schönherr, Asja Fischer, Dorothea Kolossa, and Thorsten Holz. Leveraging Frequency Analysis for Deep Fake Image Recognition. In *ICML*, pages 3247–3258, 2020. 3

- [32] Samir Yitzhak Gadre, Gabriel Ilharco, Alex Fang, Jonathan Hayase, Georgios Smyrnis, Thao Nguyen, Ryan Marten, Mitchell Wortsman, Dhruva Ghosh, and Jieyu Zhang et al. DataComp: In search of the next generation of multimodal datasets. *arXiv preprint arXiv:2304.14108*, 2023. [6](#)
- [33] Diego Gragnaniello, Davide Cozzolino, Francesco Marra, Giovanni Poggi, and Luisa Verdoliva. Are GAN generated images easy to detect? A critical analysis of the state-of-the-art. In *ICME*, pages 1–6, 2021. [2](#), [7](#), [10](#), [11](#)
- [34] Jonathan Ho, Ajay Jain, and Pieter Abbeel. Denoising diffusion probabilistic models. In *NeurIPS*, pages 6840–6851, 2020. [10](#)
- [35] Gabriel Ilharco, Mitchell Wortsman, Ross Wightman, Cade Gordon, Nicholas Carlini, Rohan Taori, Achal Dave, Vaishaal Shankar, Hongseok Namkoong, John Miller, Hannaneh Hajishirzi, Ali Farhadi, and Ludwig Schmidt. [https://github.com/mlfoundations/open\\_clip](https://github.com/mlfoundations/open_clip), 2021. [6](#)
- [36] Hyeonseong Jeon, Young Oh Bang, Junyaup Kim, and Simon Woo. T-GD: Transferable GAN-generated Images Detection Framework. In *ICML*, pages 4746–4761, 2020. [2](#)
- [37] Yonghyun Jeong, Doyeon Kim, Youngmin Ro, Pyounggeon Kim, and Jongwon Choi. FingerprintNet: Synthesized Fingerprints for Generated Image Detection. In *ECCV*, pages 76–94, 2022. [3](#)
- [38] Yan Ju, Shan Jia, Lipeng Ke, Hongfei Xue, Koki Nagano, and Siwei Lyu. Fusing Global and Local Features for Generalized AI-Synthesized Image Detection. In *ICIP*, pages 3465–3469, 2022. [2](#)
- [39] Minguk Kang, Jun-Yan Zhu, Richard Zhang, Jaesik Park, Eli Shechtman, Sylvain Paris, and Taesung Park. Scaling up gans for text-to-image synthesis. In *CVPR*, pages 10124–10134, 2023. [4](#), [10](#)
- [40] Tero Karras, Tilo Aila, Samuli Laine, and Jaakko Lehtinen. Progressive Growing of GANs for Improved Quality, Stability, and Variation. In *ICLR*, 2018. [2](#), [4](#)
- [41] Tero Karras, Samuli Laine, and Timo Aila. A style-based generator architecture for generative adversarial networks. In *CVPR*, pages 4401–4410, 2019. [4](#), [10](#)
- [42] Tero Karras, Samuli Laine, Miika Aittala, Janne Hellsten, Jaakko Lehtinen, and Timo Aila. Analyzing and improving the image quality of StyleGAN. In *CVPR*, pages 8110–8119, 2020. [4](#)
- [43] Tero Karras, Miika Aittala, Samuli Laine, Erik Härkönen, Janne Hellsten, Jaakko Lehtinen, and Timo Aila. Alias-free generative adversarial networks. In *NeurIPS*, pages 852–863, 2021. [3](#), [4](#)
- [44] Misha Konstantinov, Alex Shonenkov, Daria Bakshandaeva, Christoph Schuhmann, Ksenia Ivanova, and Nadiia Klokova. <https://www.deepfloyd.ai/deepfloyd-iff>, 2023. [4](#), [10](#)
- [45] Junnan Li, Dongxu Li, Caiming Xiong, and Steven Hoi. BLIP: Bootstrapping Language-Image Pre-training for Unified Vision-Language Understanding and Generation. In *ICML*, pages 12888–12900, 2022. [4](#)
- [46] Tsung-Yi Lin, Michael Maire, Serge Belongie, James Hays, Pietro Perona, Deva Ramanan, Piotr Dollár, and C Lawrence Zitnick. Microsoft COCO: Common objects in context. In *ECCV*, pages 740–755, 2014. [4](#), [10](#)
- [47] Bo Liu, Fan Yang, Xiuli Bi, Bin Xiao, Weisheng Li, and Xinbo Gao. Detecting generated images by real images. In *ECCV*, pages 95–110, 2022. [2](#), [7](#), [10](#), [11](#)
- [48] Sara Mandelli, Nicolò Bonettini, Paolo Bestagini, and Stefano Tubaro. Detecting GAN-generated Images by Orthogonal Training of Multiple CNNs. In *ICIP*, pages 3091–3095, 2022. [2](#)
- [49] Francesco Marra, Diego Gragnaniello, Luisa Verdoliva, and Giovanni Poggi. Do GANs Leave Artificial Fingerprints? In *MIPR*, pages 506–511, 2019. [1](#), [2](#)
- [50] Francesco Marra, Cristiano Saltori, Giulia Boato, and Luisa Verdoliva. Incremental learning for the detection and classification of GAN-generated images. In *WIFS*, pages 1–6, 2019. [2](#)
- [51] Falko Matern, Christian Riess, and Marc Stamminger. Exploiting visual artifacts to expose deepfakes and face manipulations. In *WACV Workshops*, pages 83–92, 2019. [2](#)
- [52] Midjourney. <https://www.midjourney.com/home>, 2023. [4](#), [12](#)
- [53] Yifei Ming, Ziyang Cai, Jiuxiang Gu, Yiyou Sun, Wei Li, and Yixuan Li. Delving into out-of-distribution detection with vision-language representations. In *NeurIPS*, pages 35087–35102, 2022. [2](#)
- [54] Harvey B Mitchell and Paul A Schaefer. A “soft” K-nearest neighbor voting scheme. *IJIS*, 16(4):459–468, 2001. [9](#)
- [55] Alex Nichol, Prafulla, Dhariwal Aditya Ramesh, Pranav Shyam, Pamela Mishkin, Bob McGrew, Ilya Sutskever, and Mark Chen. GLIDE: Towards Photorealistic Image Generation and Editing with Text-Guided Diff. Models. In *ICML*, pages 16784–16804, 2022. [3](#), [4](#)
- [56] Utkarsh Ojha, Yuheng Li, and Yong Jae Lee. Towards universal fake image detectors that generalize across generative models. In *CVPR*, pages 24480–24489, 2023. [2](#), [3](#), [7](#), [10](#), [11](#)
- [57] William Peebles and Saining Xie. Scalable diffusion models with transformers. In *ICCV*, pages 4195–4205, 2023. [4](#), [10](#)
- [58] Dustin Podell, Zion English, Kyle Lacey, Andreas Blattmann, Tim Dockhorn, Jonas Müller, Joe Penna, and Robin Rombach. SDXL: Improving latent diffusion models for high-resolution image synthesis. *arXiv preprint arXiv:2307.01952v1*, 2023. [3](#), [4](#), [6](#), [11](#)
- [59] Alec Radford, JongWook Kim, Chris Hallacy, Aditya Ramesh, Gabriel Goh, Sandhini Agarwal, Girish Sastry, Amanda Askell, Pamela Mishkin, and Jack Clark et al. Learning transferable visual models from natural language supervision. In *ICML*, pages 8748–8763, 2021. [2](#)
- [60] Aditya Ramesh, Prafulla Dhariwal, Alex Nichol Casey, Chu, and Mark Chen. Hierarchical text-conditional image generation with clip latents. *arXiv preprint arXiv:2204.06125v1*, 2022. [3](#), [4](#)
- [61] Robin Rombach, Andreas Blattmann, Dominik Lorenz, Patrick Esser, and Björn Ommer. High-resolution image synthesis with latent diffusion models. In *CVPR*, pages 10684–10695, 2022. [4](#)
- [62] Robin Rombach, Andreas Blattmann, Dominik Lorenz, Patrick Esser, and Björn Ommer. <https://github.com>.

- com/Stability-AI/stablediffusion, 2022. 3, 4, 6, 10, 11
- [63] Axel Sauer, Tero Karras, Samuli Laine, Andreas Geiger, and Timo Aila. StyleGAN-T: Unlocking the power of GANs for fast large-scale text-to-image synthesis. In *ICML*, 2023. 4, 10
- [64] Christoph Schuhmann, Richard Vencu, Romain Beaumont, Robert Kaczmarczyk, Clayton Mullis, Aarush Katta, Theo Coombes, Jenia Jitsev, and Aaran Komatsuzaki. LAION-400M: Open Dataset of CLIP-Filtered 400 Million Image-Text Pairs. In *NeurIPS Workshops*, 2021. 4, 6
- [65] Christoph Schuhmann, Romain Beaumont, Richard Vencu, Cade W Gordon, Ross Wightman, Mehdi Cherti, Theo Coombes, Aarush Katta, Clayton Mullis, and Mitchell Wortsman et al. LAION-5B: An open large-scale dataset for training next generation image-text models. In *NeurIPS*, pages 25278–25294, 2022. 6
- [66] Zeyang Sha, Zheng Li, Ning Yu, and Yang Zhang. DE-FAKE: Detection and Attribution of Fake Images Generated by Text-to-Image Diffusion Models. *arXiv preprint arXiv:2210.06998v1*, 2022. 2, 3
- [67] Sergey Sinitisa and Ohad Fried. Deep image fingerprint: Accurate and low budget synthetic image detector. In *WACV*, 2024. 2
- [68] Yang Song, Jascha Sohl-Dickstein, Diederik P Kingma, Abhishek Kumar, Stefano Ermon, and Ben Poole. Score-based generative modeling through stochastic differential equations. In *ICLR*, 2020. 4, 10
- [69] Chuangchuang Tan, Yao Zhao, Shikui Wei, Guanghua Gu, and Yunchao Wei. Learning on Gradients: Generalized Artifacts Representation for GAN-Generated Images Detection. In *CVPR*, pages 12105–12114, 2023. 2, 7, 10, 11
- [70] Ming Tao, Bing-Kun Bao, Hao Tang, and Changsheng Xu. GALIP: Generative Adversarial CLIPs for Text-to-Image Synthesis. In *CVPR*, pages 14214–14223, 2023. 10
- [71] Sheng-Yu Wang, Oliver Wang, Richard Zhang, Andrew Owens, and Alexei A Efros. CNN-generated images are surprisingly easy to spot... for now. In *CVPR*, pages 8692–8701, 2020. 1, 2, 6, 7, 10, 11
- [72] Zhendong Wang, Jianmin Bao, Wengang Zhou, Weilun Wang, Hezhen Hu, Hong Chen, and Houqiang Li. DIRE for Diffusion-Generated Image Detection. *ICCV*, 2023. 3, 7, 10, 11
- [73] Zhendong Wang, Huangjie Zheng, Pengcheng He, Weizhu Chen, and Mingyuan Zhou. Diffusion-GAN: Training GANs with Diffusion. In *ICLR*, 2023. 10
- [74] Mengde Xu, Zheng Zhang, Fangyun Wei, Yutong Lin, Yue Cao, Han Hu, and Xiang Bai. A simple baseline for open-vocabulary semantic segmentation with pre-trained vision-language model. In *ECCV*, pages 736–753, 2022. 2
- [75] Xingyi Yang, Daquan Zhou, Jiashi Feng, and Xinchao Wang. Diffusion probabilistic model made slim. In *CVPR*, pages 22552–22562, 2023. 3
- [76] Fisher Yu, Ari Seff, Yinda Zhang, Shuran Song, Thomas Funkhouser, and Jianxiong Xiao. LSUN: Construction of a large-scale image dataset using deep learning with humans in the loop. *arXiv preprint arXiv:1506.03365*, 2015. 4, 10
- [77] Ning Yu, Larry Davis, and Mario Fritz. Attributing Fake Images to GANs: Learning and Analyzing GAN Fingerprints. In *ICCV*, pages 7555–7565, 2019. 1, 2
- [78] Renrui Zhang, Wei Zhang, Rongyao Fang, Peng Gao, Kunchang Li, Jifeng Dai, Yu Qiao, and Hongsheng Li. Tip-Adapter: Training-free Adaption of CLIP for Few-shot Classification. In *ECCV*, pages 493–510, 2022. 2, 3
- [79] Xu Zhang, Svebor Karaman, and Shih-Fu Chang. Detecting and Simulating Artifacts in GAN Fake Images. In *WIFS*, pages 1–6, 2019. 1, 3
- [80] Kaiyang Zhou, Jingkang Yang, Chen Change Loy, and Ziwei Liu. Learning to prompt for vision-language models. *IJCV*, 130(9):2337–2348, 2022. 3
- [81] Ziqin Zhou, Yinjie Lei, Bowen Zhang, Lingqiao Liu, and Yifan Liu. ZegCLIP: Towards Adapting CLIP for Zero-shot Semantic Segmentation. In *CVPR*, pages 11175–11185, 2023. 2